Photoelectron angular distributions in photodetachment from P⁻

O. Windelius,[1,2] J. Welander [ORCID],[2,*] A. Aleman,[2] D. J. Pegg,[3] K. V. Jayaprasad,[4] S. Ali,[5] and D. Hanstorp[2]

[1]*Department of Physics, Chalmers University of Technology, SE-412 96 Gothenburg, Sweden*
[2]*Department of Physics, University of Gothenburg, SE-412 96 Gothenburg, Sweden*
[3]*Department of Physics, University of Tennessee, Knoxville, Tennessee 37996, USA*
[4]*International School of Photonics, Cochin University of Science and Technology, Kalamassery, Kochi-682022 Kerala, India*
[5]*Department of Physics, University of Gujrat, Jalalpur Jattan Road, Gujrat 50700, Pakistan*

The angular distributions of electrons ejected in laser photodetachment of the P⁻ ion have been studied in the photon energy range of 0.95–3.28 eV using a photoelectron spectrometer designed to accommodate a source consisting of collinearly overlapping photon and negative ion beams. We observe the value of the asymmetry parameter β starting at zero near the threshold, falling to almost −1 about 0.5 eV above the threshold and eventually rising to a positive value. The experimental data has been fitted to a simplified model of the Cooper-Zare formula which yields a qualitative understanding of the quantum interference between the outgoing s and d waves representing the free electron. The present results are also compared with previous results for other elements involving p-electron photodetachment.

I. INTRODUCTION

Negative ions are unique quantum systems with several properties that are interesting from a fundamental point of view [1,2]. The independent-particle approximation [3,4], which adequately describes the structure of atoms and positive ions, fails to explain the formation of many atomic negative ions [5,6]. In such systems, correlation between the electrons is relatively more pronounced and is responsible for the binding of an additional electron to the atomic core. For those atomic ions that are stably bound, the relatively weak binding potential supports with only a few exceptions a single bound state [7]. The enhanced role played by electron correlation in the structure and dynamics of negative ions provides a means of testing theoretical models that go beyond the independent-electron model [8,9].

The primary method for experimentally studying negative ions is the bound-free process of photodetachment [10]. Here, the energy and angular momentum of a photon is transferred to a negative ion, which subsequently breaks up into a free electron and a neutral atom. The initial energy and angular momentum of the photon are conserved

and shared by the two particles in the final state. A measurement of the energy of a free photoelectron permits a determination of the binding energy of the bound electron in the negative ion. Similarly, a measurement of the angular distribution of the ejected photoelectrons yields information on the symmetry of the negative ion prior to photodetachment.

In the case of plane-polarized light in the electric dipole approximation and randomly polarized target ions, the photoelectron angular distribution (PAD) takes the form [11]

$$\frac{d\sigma}{d\Omega} = \frac{\sigma}{4\pi}\left[1 + \frac{\beta}{2}(3\cos^2\theta - 1)\right], \qquad (1)$$

where σ represents the total cross section and $d\sigma/d\Omega$ is the differential cross section. The asymmetry parameter β contains all the information needed to completely characterize the photoelectron angular distribution. The angle θ refers to the angle between the polarization vector of the light and the momentum vector of the photoelectron. In general, β is photon energy dependent.

A free electron can be represented in the final state of photodetachment by two partial waves whose amplitudes and phases are determined by the radial matrix elements describing the bound-free transition. In a central potential, a model describing the asymmetry parameter with an implicit energy dependence in the transition amplitudes and phases into the partial waves of the final state has been derived by Bethe [11]. The model is more commonly known as the Cooper-Zare formula from the work of Cooper and Zare [12,13] that generalized the model to also be applicable to many-electron

*jakob.welander@gu.se

systems. The formula reads

$$\beta = \frac{l(l-1)R_{l-1}^2 + (l+1)(l+2)R_{l+1}^2 - 6l(l+1)R_{l-1}R_{l+1}\cos(\delta_{l+1}-\delta_{l-1})}{(2l+1)\left[lR_{l-1}^2 + (l+1)R_{l+1}^2\right]}. \tag{2}$$

Here, l is the orbital angular momentum quantum number of the electron in the bound state prior to photodetachment, $R_{l\pm1}$'s are the radial matrix elements for the allowed dipole transitions, and $\delta_{l+1} - \delta_{l-1}$ is the residual phase difference between the outgoing partial waves representing the photoelectron in the final state. According to the dipole selection rules, the photoejection of a bound electron in a nonzero orbital angular momentum state l, will produce a free electron that can be represented in the final state by partial waves with an angular momentum $l \pm 1$. The overlap of the two partial waves with different amplitudes and phases will lead to interference, which can be investigated by measuring the photon energy dependence of the asymmetry parameter that characterizes the photoelectron angular distribution.

A calculation of β using the Cooper-Zare formula requires the evaluation of the radial matrix elements $R_{l\pm1}$, which is a nontrivial task. Hanstorp *et al.* [14] circumvented this difficulty by making certain assumptions that simplified the Cooper-Zare formula and applied it to the case of the final-state interference of s and d waves following the ejection of a p orbital electron in the initial state of an O$^-$ ion. In their approximation, it is assumed that the final-state wavelength is large compared with the size of the initial state. In addition, the interaction between the free electron and the residual atom in the final state is assumed to be negligible. Under these conditions, $R_{l\pm1}$ is proportional to $k^{l\pm1}$ for the two continuum channels where k is the wave number of the free electron. These matrix elements determine the amplitudes of the partial waves. The simple dependence on k originates from the Wigner threshold law [15], which typically is valid only in the near-threshold region.

In the case of interfering s and d waves, the ratio of the two radial matrix elements R_2/R_0 is proportional to k^2. This can be written as $R_2/R_0 = A_2\varepsilon$, where $\varepsilon = k^2$ is the energy of the free electron and A_2 corresponds to the relative size of the two matrix elements. In addition, the residual phase shift between the outgoing partial waves is assumed to be a constant independent of the photon energy. For the case of photodetachment of a p-orbital electron, the simplified model can then be written as

$$\beta = \frac{2A_2\varepsilon(A_2\varepsilon - 2c)}{1 + 2A_2^2\varepsilon^2}, \tag{3}$$

where $c = \cos(\delta_2 - \delta_0)$. In the work of Hanstorp *et al.* [14] the asymmetry parameter for O$^-$ photodetachment was measured at five photoelectron energies between 0.2 and 1.2 eV. Initially, to simplify the analysis, the difference of the residual phase shifts between the two outgoing waves was set to zero, making $c = 1$. A_2 was then adjusted so that the minimum in the curve of the spectral dependence of the asymmetry parameter coincided with experimental data. The inclusion of the c parameter in the fit results in a slightly better adjustment, yielding a value of $c = 0.925$. The model exhibited good agreement over a large energy range despite the fact

that the main assumption $R_2/R_0 = A_2\varepsilon$ originates from the Wigner threshold law which is known to be valid only in a region just above threshold. This can be explained by the fact that the model only includes the ratio of the matrix elements R_2/R_0 and not their absolute values. The model is, therefore, applicable even at energies above the range of the validity of the Wigner law, provided that the deviation from the k^{2l+1} behavior is the same for the s and d waves.

The model used to describe PADs, as presented in Eq. (3), is strictly valid only in the atomic case where the valence electron of the negative ion can be assigned a discrete value of angular momentum. In contrast, the wave function of the valence electron in a molecule is normally described as a mixture of angular momenta, such as $s - p$ or $p - d$ mixing. The fact that, e.g., detachment of an s-electron occurs with a constant $\beta = 2$ whereas detachment of a p-electron gives the characteristic energy dependence as described by Eq. (3), can then be used to investigate the degree of mixing in molecular systems [16]. This use of the model presented as Eq. (3) to analyze molecular negative ions motivates a detailed study of its behavior in the pure case of atomic systems.

The primary motivation for the present paper on P$^-$ photodetachment is to investigate the validity of the approximation made by Hanstorp *et al.* [14] over a range of photon energies larger than that used in the O$^-$ experiment. To achieve this goal, we photodetached electrons from the P$^-$ ion and studied the spectral dependence of the asymmetry parameter over the range of photoelectron energies of 0.2–2.5 eV. The only previous experimental investigation of the asymmetry parameter of P$^-$ covered the more limited energy range of 1.17–1.96 eV [17]. P$^-$, with an electron ground-state configuration of [Ne] $3s^23p^4\,^3P_2$, was selected for this paper since it can be efficiently produced in our ion source, and at the same time its small electron affinity (EA) allows an investigation over a large range of photoelectron energies. A schematic showing the energy levels in P$^-$ and the lowest levels in P are shown in Fig. 1.

In the present experiment we are also introducing an apparatus designed to measure photoelectron angular distributions with collinear interacting ion and laser beams. Almost all previous asymmetry parameter measurements have employed a crossed beams interaction geometry in which a beam of negative ions is crossed perpendicularly with a linearly polarized laser beam. In such an arrangement, the spatially well-defined interaction region permits the ejected photoelectrons to be efficiently collected and energy analyzed using either an electrostatic analyzer [18] or a velocity mapping technique [19]. However, the number of photodetachment events are severely limited by the relatively small interaction volume. The latter can be increased considerably if the laser and ion beam interact in a collinear geometry. This advantage is, however, offset by the difficulty of collecting photoelectrons from such an extended linear source. Nevertheless, the intrinsically low density of negative ions in a beam source makes the collinear
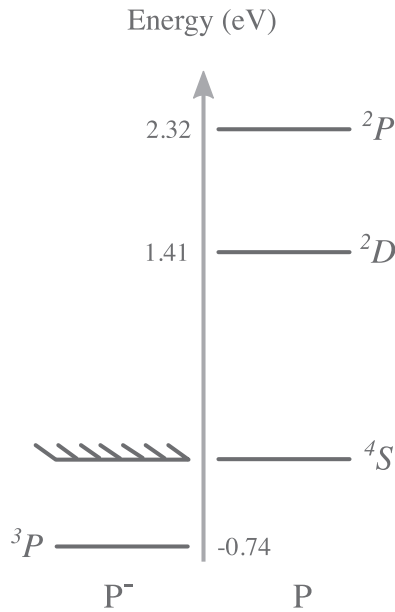
Energy (eV)

FIG. 1. Energy diagram of P^- and the lowest levels of P.

beam geometry an attractive prospect. The first measurements of photoelectron angular distributions using a collinear geometry were made by Hanstorp *et al.* [14] in 1989. The success of this experiment inspired the development of the present apparatus, which has been named by the acronym PEARLS (PhotoElectron Angle-Resolved Linear Spectrometer). PEARLS is primarily designed for use at synchrotron

facilities, where beam time is at a premium and the rotation of the polarization vector of the radiation is not always a viable option. Fluxes from synchrotrons and lasers are very different. For example, synchrotron sources typically produce $\sim 10^{14}$ photons/s, much less than the $\sim 10^{17}$ photons/s generated by our amplified lasers. Hence, the long interaction region is a necessity when using synchrotrons as light sources in order to accumulate sufficient data within a typical limited time allocation. The present experiment, which involves lasers as the photon sources, demonstrates the functionality of the spectrometer. A detailed account of the PEARLS apparatus can be found in a recent publication by Windelius *et al.* [20] where the hardware and results from test experiments involving photoelectron angular distributions with known asymmetry parameters are presented.

II. EXPERIMENTAL METHOD

The experiment was performed at the Gothenburg University Negative Ion Laser LAboratory (GUNILLA) facility [21]. A schematic of the apparatus is shown in Fig. 2. In the present experiment, a stable beam of P^- ions was produced in a sputter ion source (Peabody PS120) using iron phosphide as the cathode material.

The ions exiting the source were accelerated to an energy of 6 keV and focused into a beam using a combination of deflection plates, Einzel lenses, and a quadrupole triplet. The ion beam was mass selected using a $90°$ sector magnet. An additional number of ion-optical elements were used to transport the essentially monoenergetic and unidirectional beam through the remaining apparatus. A vacuum in the 10^{-7}-mbar
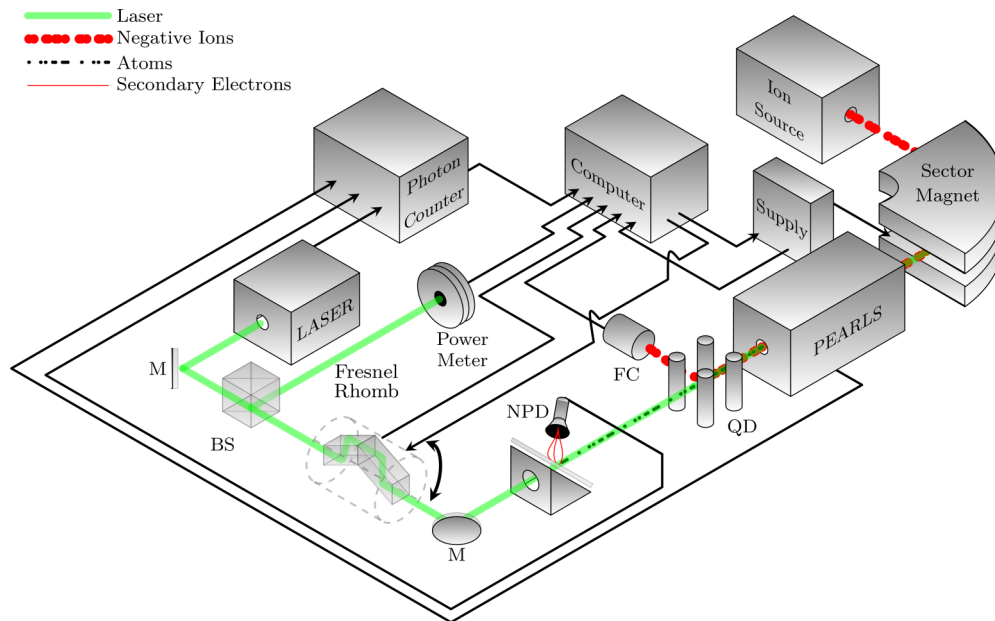
FIG. 2. The experimental setup at the GUNILLA facility in a schematic. A beam of negative ions produced in the ion source undergo mass selection in the sector magnet. The selected isobaric beam is then guided into the interaction region of PEARLS where photoelectrons are detected (see Fig. 3). Negative ions surviving detachment are directed into a Faraday cup (FC) by a quadrupole deflector (QD). Residual atoms formed in detachment processes travel further downstream onto a neutral particle detector (NPD). Light from the laser is directed by mirrors (M) into PEARLS where it is overlapped with the ion beam. A fraction of the laser beam is directed onto a power meter by means of a beam splitter (BS). The direction of polarization of the laser beam is controlled by a Fresnel rhomb. The black arrows indicate the connections to devices in the computer-controlled data-acquisition system.

TABLE I. Asymmetry parameters for P^- photodetachment in the photon energy range of 0.95–3.28 eV (1310–378 nm). λ is the laser wavelength, E_p is the photon energy, and E_k is the photoelectron energy. β_{meas} is the measured asymmetry parameter. The column labeled Laser, finally, shows the type of laser used in the experiment.

λ (nm)	E_p (eV)	E_k (eV)	β_{meas}	Laser
378	3.28	2.53	0.32(5)	Ti:sapphire
400	3.10	2.35	0.27(14)	Ti:sapphire
405	3.06	2.32	0.31(4)	Ti:sapphire
422	2.94	2.19	0.24(12)	Ti:sapphire
532	2.33	1.58	−0.02(2)	Yttrium aluminum garnet (YAG)[a]
700	1.77	1.02	−0.29(1)	Optical parametric oscillator (OPO)
807	1.54	0.79	−0.47(4)	Ti:sapphire
841	1.47	0.73	−0.51(5)	Ti:sapphire
1064	1.17	0.42	−0.71(6)	YAG[b]
1150	1.08	0.33	−0.72(29)	OPO
1310	0.95	0.20	−0.22(10)	OPO

[a]A laser with a 5-kHz repetition rate.
[b]A laser with a 20-Hz repetition rate.

range was maintained in the beamlines in order to minimize the destruction of the P^- ions in collisions with molecules of the residual gas.

The ion beam was directed to and through the PEARLS chamber, housing the interaction region, which was located at the end of a 2-m drift tube. The interaction region was defined by two 3-mm apertures placed at the entrance and exit of PEARLS, respectively.

Downstream from the PEARLS chamber, the particle beam passed through a quadrupole deflector which was used to direct the remaining negative ion component of the beam into a Faraday cup, yielding ion currents on the order of 1 nA.

Several different pulsed lasers, listed in Table I in Sec. III, were used to generate a rather wide range of photon energies. Common to all laser outputs were bandwidths $\leqslant 6$ GHz. A variable intensity filter consisting of two crossed polarizers was used to attenuate the laser beam to avoid detector saturation. The pulse energy that could be used to avoid saturation, which depends on the magnitude of the photodetachment cross section, was typically on the order of 100 μJ. The direction of the linear polarization of the laser was manipulated using a Fresnel rhomb prior to the last guiding optics directing the laser into the interaction region.

The interaction region enabled collinear overlap between the ion beam and the co-propagating laser beam. The main interaction studied was photodetachment of the negative ion beam with free electrons and neutral atoms as the resulting products. The pressure in the interaction region was kept at 10^{-8} mbar in order to reduce competing background effects arising from collisional detachment.

Residual atoms produced in photodetachment and collisional detachment processes proceeded further downstream where they were detected using a neutral particle detector [22]. In this detector, secondary electrons were produced when the neutral particles struck a tilted glass plate. These secondary electrons were focused onto a channel electron multiplier (CEM) and counted.

Electron emission from photodetachment events in the interaction region constituted the signal in the measurements that was conducted using the newly commissioned spectrometer PEARLS [20]. The design and function of PEARLS has

been described in detail by Windelius *et al.* [20]. In short, the linear source of photoelectrons produced in the region of the overlapping laser and ion beams is surrounded by two linearly aligned 11-cm long graphite tubes with a square cross section [Fig. 3(a)]. Graphite was chosen to minimize electrostatic patch fields on the surfaces. The whole spectrometer was placed inside a μ-metal shield. The electron emission inside the graphite tube, hence, occurred in an essentially field-free environment. Photoelectrons created inside the graphite tubes are able to exit through 14 small and evenly spaced holes placed on each of the four sides of the tubes. Electrons not passing through the holes are absorbed by the grounded graphite tube. Electrons exiting the holes pass first through a filter consisting of a fine copper mesh which can be biased to suppress low-energy electrons. This filter was used for photon energies $\geqslant 2.33$ eV to block low-energy photoelectrons associated with detachment processes involving excited states of the residual P atom. After passing through the filter, the electrons entered a rectangular copper box in which an electric field guides the electrons into a CEM. Four CEMs were placed on a single plane as shown in Fig. 3(b). PEARLS consists of four such planes of detectors, giving a total of 16 CEMs. In the
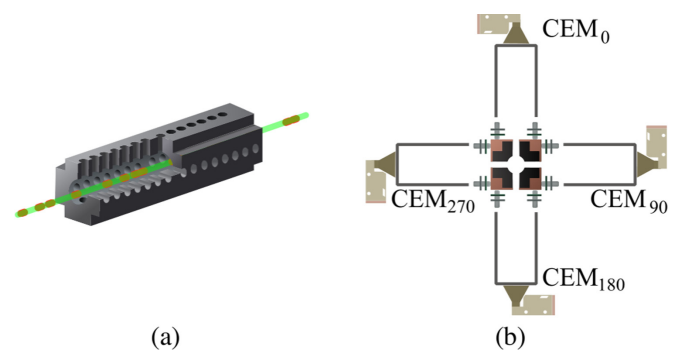
FIG. 3. (a) shows one of the two graphite tubes inside PEARLS within which the ion and photon beams interact. The photoelectrons escape through the small holes on the sides of the tube or are absorbed by the graphite surfaces. (b) Cross section of one detector plane of PEARLS used in the current experiment.

present experiment, however, only one plane with four CEMs was employed.

The output from each CEM was amplified with a preamplifier and sent to a photon counter that was used for gating and acquisition. The signal-to-background ratio was enhanced by using a time-gated detection that was triggered by the laser pulse. A time window of 10 ns was used, which is slightly less than twice the rise time of the CEMs. A second time window placed 100 ns after the photoelectron signal was used to record electrons from collisional background events. This background was subtracted from the signal, although it was found to be essentially negligible. The rate of neutrals was simultaneously recorded in order to monitor the overlap between the laser and the ion beams. Additionally, the ion current was monitored during measurements for the same purpose. The ion and laser beams as well as their overlap showed stable conditions over the time required to measure the angular distribution at a single laser wavelength.

The photoelectron angular distribution, i.e., photoelectron yields as a function of the angle between the polarization vector and the electron momentum vector, can be measured either by rotating the polarization vector of the laser using a Fresnel rhomb and measure the yield of collected photoelectrons in any of the CEMs or by keeping the polarization vector fixed and measure the photoelectron yields in two orthogonal detectors situated, for example, at $0°$ and $90°$ or $180°$ and $270°$ [20]. For the case of static polarization it was necessary to verify an equal counting efficiency of the CEMs in an orthogonal set. This was achieved by detecting isotropic emitted electrons from collisional detachment of the ion while the laser was off. Such a procedure allows the experimental parameters to be adjusted to get an equal electron yield in each of the four detectors. In this paper, both the method of rotating the polarization vector and the method keeping it fixed were applied to measure angular distributions.

III. RESULTS

Figure 4 is a polar plot that shows the angular distribution of photoelectrons ejected from P^- using a photon energy of 3.06 eV ($\lambda = 405$ nm). The polar angle refers to the angle between the polarization direction and the direction of electron momentum in the laboratory frame. The range from $0°$ to $180°$ was mapped out in increments of $10°$ by rotating the direction of polarization of the laser. The error bars show the statistical uncertainty of one standard error.

The photoelectron yields at each angle were determined from the signals registered in a single plane detector set as shown in Fig. 3(b). A value of the asymmetry parameter of $\beta = 0.31 \pm 0.04$ was obtained by fitting the data in Fig. 4 to the model described by Eq. (1).

The present paper extends the previous photoelectron angular distribution measurement on P^- [17] to photon energies in the range of 0.95–3.28 eV (1310-378 nm). The electron affinity of phosphorus is 0.746 607(10) eV [23] corresponding to photoelectron energies from 0.2 to 2.53 eV. Column 4 in Table I shows the measured values of the asymmetry parameter (β_{meas}). The uncertainties shown on the data points are the statistical uncertainties which vary considerably between the data points. This is primarily caused by the fact that the
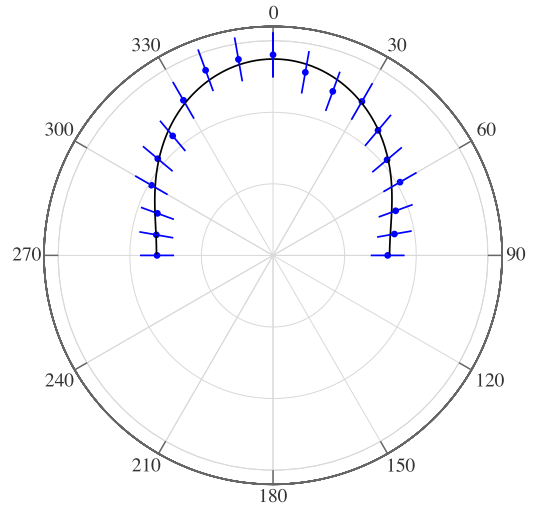
FIG. 4. Measured photoelectron yields as a function of the angle of polarization of the laser light with a photon energy of 3.06 eV. The solid line, which is a fit using Eq. (1), produces a value of the asymmetry parameter of $\beta = 0.31 \pm 0.04$. This value needs to be corrected for effects associated with kinematics and the finite spread in acceptance angles. For more details, see the text.

data were recorded with lasers operating at different repetition rates, ranging from 10 Hz to 5 kHz. This resulted in different data-acquisition rates leading to different statistical uncertainties of the data points.

The values shown in Table I have been affected both by the kinematic effect and by the nonzero acceptance angle of the spectrometer [20]. A kinematic correction is necessary because the photoelectrons are ejected from moving ions. Thus, a transformation between angles in the ion and the laboratory reference frames must be applied. The angle between the electron momenta in the two frames of reference is a function of the ion velocity and the velocities of the detached electron in each frame. The asymmetry parameter can be corrected for the kinematic effect ($\beta_{\text{kin,corr}}$) by using the equation,

$$\beta_{\text{kin,corr}} = \frac{\beta_{\text{meas}}}{1 - \frac{v_i^2}{v_e^2}(1 - \beta_{\text{meas}}/2)}. \tag{4}$$

Here, v_i is the velocity of the ions in the laboratory frame, v_e is the velocity of the emitted electron in the center-of-mass frame, and β_{meas} is the measured asymmetry parameter. For instance, by direct application of Eq. (4) the measured value of $\beta = -0.51(5)$ at 841 nm gives a kinematically corrected value of $-0.62(6)$.

Furthermore, the finite size of the exit holes together with the extended linear source allows electrons within a small range of emission angles to be detected by the CEMs. The combined effects of kinematics and the finite spread in acceptance angles of the spectrometer were investigated by simulating the emission and detection of electrons using the ray-tracing software SIMION [24]. Details of this correction procedure can be found in the publication on PEARLS by Windelius *et al.* [20]. We found that the effect of the kinematics is causing the main difference between the measured and the corrected data. The effect of the finite acceptance angle gives only a small correction for the low-energy points

whereas it is negligible for the higher-energy points. As an example, for the point at 841 nm, the value $-0.62(6)$, corrected only for the kinematic effect only, is changed to $-0.63(6)$ when the correction for the nonzero acceptance angle is included in the analysis.

The obvious method to perform the analysis of the data would be to first correct each datapoint for both the kinematic effect and the nonzero acceptance angle. However, two data points then yield values < -1, namely, the points at $\lambda = 1064$ and $\lambda = 1150$ nm, although they both coincide with -1 within one standard error. This is caused by the fact that we do get a signal at $\theta = 0°$, even when $\beta = -1$ (i.e., where the distribution is a pure $\sin^2 \theta$). Statistical fluctuations after removal of the background signal can then give us numerical values of β that are smaller than -1, but β can only take on values in the range of $[-1, 2]$. Therefore, we are unable to use Eq. (3) to extract the A_2 and c parameters. Instead, we transform Eq. (3) in terms of the measured values β_{meas} by taking into account the kinematic correction through Eq. (4) and, thus, find the model parameters A_2 and c by fitting to the corrected model. Hence, we do not include the small effect associated with the nonzero acceptance angle in the following analysis. The new equation reads

$$\beta_{\mathrm{meas}} = \frac{2\varepsilon A_2(x^2 - 1)(\varepsilon A_2 - 2c)}{\varepsilon^2 A_2^2 x^2 - 2\varepsilon^2 A_2^2 - 2\varepsilon A_2 x^2 c - 1}, \qquad (5)$$

where

$$x(\varepsilon) = \frac{v_i}{v_e} = \frac{m_e}{m_i} \frac{eU}{\varepsilon}.$$

Here, m_e and m_i are the electron and ion masses, respectively, U is the ion acceleration potential, and e is the electron charge. Note that Eq. (5) represents the asymmetry parameter as a function of the photoedetachment energy measured in the laboratory reference frame. Equation (5) reduces to Eq. (3) when the kinematic effect is neglected ($x \sim 0$ for $v_e \gg v_i$). Finally, Eq. (5) becomes zero at the additional condition $x(\varepsilon)^2 = 1$, which corresponds to the limit where no electron can be detected due to the kinematic effect.

Possible systematic uncertainties and our procedure to correct for the kinematic effect and the nonzero acceptance angle were investigated by measuring the angular distribution of electrons ejected in the photodetachment of the Ag$^-$ ion [20]. In this case the asymmetry parameter β is 2 for all photon energies. Stray electric or magnetic fields in the interaction region could affect the trajectories of the emitted electrons. However, such fields would not change the trajectory of a photoelectron in any specific direction and would, therefore, be manifested as a statistical uncertainty in an angular distribution measurement. Reflections of the electrons on walls of the inside of the graphite tubes and a nonperfect linear polarization of the laser beam would both change the angular distribution to be more isotropic. The experiment of Ag$^-$, yields a measured value of $\beta = 1.86 \pm 0.12$, which agrees within the uncertainties with the simulated value. Our experimental values also agree very well with the values for P$^-$ of Covington *et al.* [17]. Furthermore, the same type of spectrometer was used to measure the angular distribution in O$^-$ [14]. These data were later confirmed by the very precise measurement performed by Génévriez *et al.* [25]. Hence, we

have shown that the systematic uncertainties are negligible compared with the rather large statistical uncertainties.

Figure 5 shows the values of the measured (green inverted triangles) values of the asymmetry parameter presented in column 4, Table I, along with the results of Covington *et al.* [17] (blue squares). The solid black line represents a weighted least-squares fit to Eq. (5) using our values of β_{meas}. The fitting procedure was performed by using A_2 and $d = \delta_2 - \delta_0$ as fitting parameters. The parameter c was then obtained by the relation $c = \cos(d)$. This yields the fitting parameters $A_2 = 1.15(26)$ eV^{-1} and $c = 0.87^{+0.11}_{-0.21}$. The deviation from the curve is largest at low energies. This is to be expected since the statistical uncertainties at low energies are the largest. In addition, at these energies the effect of kinematics and nonzero acceptance angle reach their maximum values and furthermore, the presence of stray electric and magnetic fields have their most significant influence on the electron trajectories in the spectrometer.

The models of Eqs. (3) and (5) assume that the phase difference between the two waves is a constant of energy. This is, of course, a simplification. Instead, as a more realistic model one could rather use a phase which is proportional to $\sqrt{E_k}$. A fit to such a model is plotted as a black dashed line in Fig. 5. As shown, the two models give quite similar fits to the experimental data. The R^2 parameters of the two fits are essentially the same, so our experiment cannot distinguish between the two models. We can use the values of A_2 and c derived from Eq. (5) to plot the angular dependence function in the center-of-mass frame [Eq. (3)]. This is plotted with a solid blue line for the case when the phase is a constant, and with a blue dashed line for the case when the phase is considered proportional to $\sqrt{E_k}$.

IV. DISCUSSION

The general behavior of PADs, well established by Cooper and Zare, is described by Eq. (2). This model can be simplified under a Wigner-like approximation [14] expressed as Eq. (3). The basis of this model can be interpreted in the following manner in the case of p-electron photodetachment. In the final state, the free electron can be represented by s- and d-partial waves. Near threshold, the centrifugal barrier suppresses the d wave leading to an angular pattern dominated by an isotropic s-wave distribution ($\beta \approx 0$). As the energy of the photons increases the d wave will start to overcome the centrifugal barrier. The two emitted waves will in the asymptotic limit and in the absence of resonances give rise to a phase shift of approximately $l\pi/2$. As a result, the s and d waves produced in the photodetachment of a bound p-electron will interfere destructively giving a negative value of the β parameter [26]. The destructive interference increases until β reaches a characteristic minimum where the depth depends on the value of the parameter c in Eq. (3). The waves are in complete destructive interference along the polarization axis at the minimum if $\beta = -1$, i.e. $c = 1$, corresponding to the residual phase difference $\delta_2 - \delta_0 = 0$. This is a pure quantum effect which cannot be explained classically. However, Mabbs *et al.* explain the mechanism of the destructive interference with a mathematical derivation from a partial-wave approach for the photodetachment case of iodine [27]. A wide range
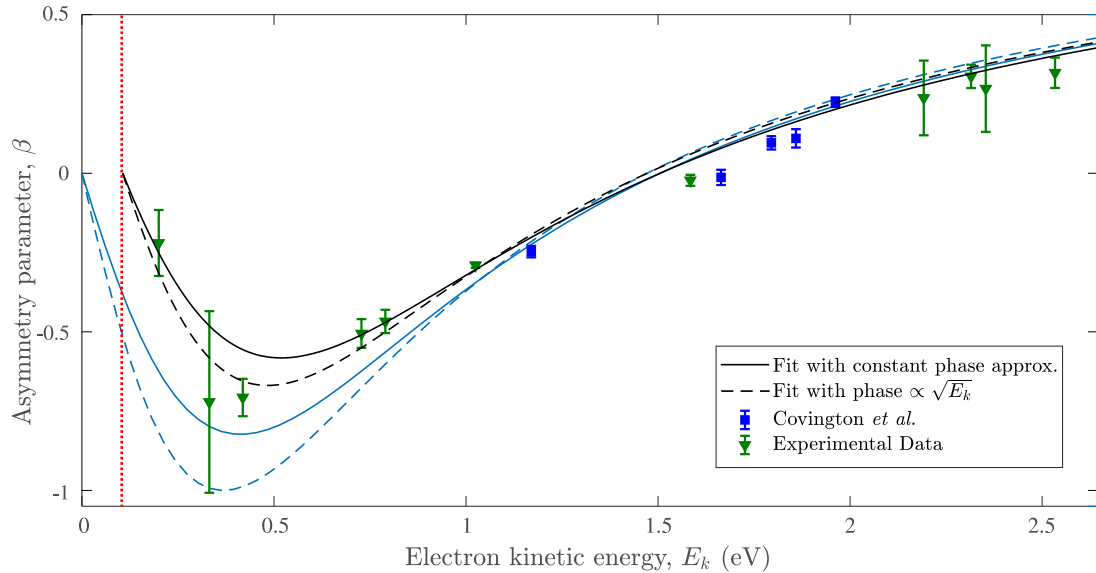
FIG. 5. Plot of the experimental asymmetry parameters as a function of the photoelectron energy. Green inverted triangles represent the measured values. The blue squares represent the previous results of Covington et $al.$ [17]. The solid and dashed black lines are the results of fitting the measured data β_{meas} to Eq. (5) using a constant phase approximation and a phase proportional to $\sqrt{E_k}$, respectively. The dotted vertical red line marks the condition $x^2 = 1$ which represents the detection limit imposed by the kinematic effect. Finally, Eq. (3) is plotted in blue (gray) using the parameters extracted from the respective black fitting curves for both phase models (the solid line for the constant phase approximation and the dashed line for the model with a phase proportional to $\sqrt{E_k}$ model). The Covington data points were not used in the fit.

of experiments [17,25,28–31] has shown that c is close to 1 for p-electron photodetachment of negative ions. At energies beyond the minimum, the d wave becomes increasingly dominant, approaching the asymptotic limit of $\beta = 1$.

In photoionization of neutral or positively charged systems, the escaping electron experiences a long-range Coulomb interaction which induces an additional phase shift of approximately $l\pi$ [26]. As a consequence, the two waves will interfere positively along the laser polarization axis giving a positive value of β [32]. The photon energy at which β reaches its minimum value for p-electron photodetachment depends primarily on the value of the A_2 parameter and the minimum moves towards higher energies as A_2 decreases. Under the assumptions of this model, A_2 may be interpreted as a measure of the spatial extension of the wave function of the negative ion. Aravind et $al.$ [33] used the data of Covington et $al.$ [17] to extract $A_2 = 0.94$ eV^{-1} and $c = 0.75$, but they did not quote any uncertainties. We also performed such a fit to their data, obtaining very similar values. However, the uncertainties became larger than the values themselves, making such a fit irrelevant. This is not unexpected since all the data points of Covington et $al.$ were recorded at energies where β tends towards its asymptotic value. This makes the results insensitive to the determination of the position and depth of the negative part of the curve describing the spectral dependence of the asymmetry parameter. Hence, by using our extended energy range we were able to better determine the fitting parameters. As a result, the minimum value of β was found to occur at a lower energy and becoming considerably closer to $\beta = -1$, implying almost complete destructive interference in P$^-$ along the polarization axis for the outgoing waves.

As stated earlier, there have been several measurements of the angular distributions of a free electron ejected in the p-electron photodetachment of atomic negative ions. In Fig. 6 we tabulate the fitting parameters obtained for those measurements [17,25,28–31] in the literature that have a sufficient number of data points to make a meaningful fit using Eq. (3). The uncertainty limits are included if they have been quoted. Our present result for P$^-$ is also included in the figure.

Let us now discuss the fitting parameters beginning with the c parameter. The values presented in Fig. 6 show that the residual phase difference of the represented elements from the four groups are nearly the same with a value of $c \approx 0.9$. Prior to our paper, P$^-$ was here an exception with a published value of $c = 0.75$. However, the new value of $c = 0.87$ falls into the pattern of other elements with the value of c being essentially a constant. This indicates that the conditions for the escaping electron is producing the same phase difference independent of the residual atom.

In contrast, the A_2 parameter is seen to vary significantly for the elements shown in Fig. 6(a). This variance can be explained by the fact that the A_2 parameter scales with the size of the negative ion. The size of the negative ion is a property which is difficult to determine, contrary to the electron affinity which can be determined with very high accuracy. However, it is expected to be inversely related to the electron affinity since a larger affinity corresponds to a more tightly bound electron and vice versa. The plot shown in Fig. 6(b) shows that the A_2 parameter does indeed scale inversely with the electron affinity.

In the present paper we have focused on the energy dependence of the asymmetry parameter describing the angular
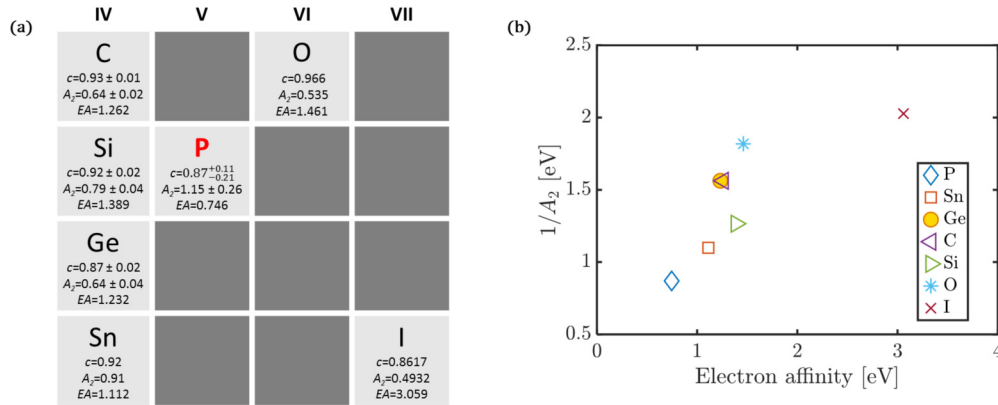
FIG. 6. (a) shows the c and A_2 parameters and the electron affinities of a number of elements for which photoelectron angular distribution measurements have been published [25,28,30,31]. Uncertainties are included in all cases where they are available. (b) shows a plot of the inverse of the A_2 parameter for the data set of (a) against their corresponding EA.

distribution of electrons emitted in the photodetachment of atomic negative ions in their ground state. In this simple case, the energy dependence can be used to get information on the symmetry of the wave function describing the initial state of the ion. In a molecule, on the other hand, the situation is much more complex. Here, the electronic wave function can be of mixed character. Khuseynov *et al.* [16], Sanov [34], and Grumbling and Sanov [35] have applied Eq. (3) in order to extract the character of the orbital mixing from PAD data. In their analysis of PADs of molecular negative ions they assume that the c parameter is 1. In the case of simultaneous s and p detachment, the mixing factor can then be determined by fitting a linear combination of a pure s and a pure p contribution. However, we have in the present paper shown that the value of the c parameter is rather $c \approx 0.9$. By using this value a more realistic determination of the mixing in the molecular negative ion could be obtained. Hence, the result from studies of atomic negative ions where the angular momentum of the valence electron is known could be used in the analysis of molecular negative ions.

V. SUMMARY AND CONCLUSIONS

Angular distributions of photoelectrons emitted in the photodetachment of P^- have been measured over a wide spectral range using a collinear spectrometer (PEARLS). Specifically, we have studied how the asymmetry parameters characterizing the angular distributions vary with photon energy. In the analysis we have used a simplified version of the Cooper-Zare formula to extract model parameters that describe the dynamics of the process. This model assumes that the relative amplitudes of the two outgoing waves follow the Wigner law and that their residual phase difference is a constant. The values of the fitting parameters obtained in the present experiment differ from those obtained in a previous measurement that involved a narrower spectral range limited to the asymptotic region of the asymmetry parameter plot. We have observed that the values of the model fitting parameters are essentially determined by those data points that are close to the photodetachment threshold region. By combining the present results with previous published results that have been

conducted over a sufficiently large spectral range, we can make a general statement. It appears that for photodetachment of atomic negative ions with valence electrons in a p orbital, the value of the model fitting parameter is $c \approx 0.9$. Furthermore, we find that the A_2 parameter, which scales with the size of the negative ion, is inversely related to the electron affinity. This is consistent with the fact that a smaller negative ion means that the electron is closer to the core which gives a larger electron affinity. In the present paper we have shown that by studying the variation of asymmetry parameters over a large spectral range, one can obtain a more detailed description of the fundamental process arising when a negative ion breaks up following the absorption of a photon. The present result together with earlier results of Fig. 6(a) supports the validity and applicability of the model presented in Eq. (3) as a special adaption of the Cooper-Zare model under Wigner assumptions. Short-range interactions due to many-body effects remain as an interesting subject for further investigation. The nature of the formation and destruction of atomic negative ions has not been studied to the same extent as atoms and positive ions. We believe that experimentally determined PADs arising from the photodetachment of atomic negative ions can be used as a probe to retrieve valuable information about the nature of the binding forces in negative ions. The model we use to describe the angular dependence of the asymmetry parameter only applies to atomic negative ions. However, the simplicity of this model makes it applicable to determine the degree of mixing of angular momentum contributions in the case of molecular negative ions. Our improved data of the pure case of an atomic negative ion will here be of great value. We hope that this paper motivates further theoretical and experimental investigations to support the analysis presented here.

The motivation for the construction of PEARLS was that it should be used for photoionization studies of positive or negative ions at synchrotron radiation facilities. The collinear geometry to overlap ion and laser beams in order to enhance the interaction volume will then be essential. In the present paper, when we have used lasers as the radiation source, it was sufficient to use a single detector plane containing four CEMs in order to achieve sufficient signal levels. When placed at a synchrotron site, all four detector planes will be utilized and,

hence, a total of 16 CEMs will collect the signal. This will give an interaction volume two orders of magnitude larger than when crossed photon and ion beams are applied. Furthermore, the design and geometry allow even more detector planes to be added, limited only by financial constraints and the available laboratory space.

[1] D. J. Pegg, Rep. Prog. Phys. **67**, 857 (2004).

[2] B. M. Smirnov, *Negative Ions* ((McGraw-Hill, New York/London 1982).

[3] D. R. Hartree and W. Hartree, Proc. R. Soc. A. **150**, 9 (1935).

[4] J. C. Slater, Rev. Mod. Phys. **35**, 484 (1963).

[5] R. Wildt, Astrophys. J. **90**, 611 (1939).

[6] C. F. Fischer, J. B. Lagowski, and S. H. Vosko, Phys. Rev. Lett. **59**, 2263 (1987).

[7] T. Andersen, H. K. Haugen, and H. Hotop, J. Phys. Chem. Ref. Data **28**, 1511 (1999).

[8] M. Y. Amusia, G. F. Gribakin, V. K. Ivanov, and L. V. Chernysheva, J. Phys. B: At., Mol. Opt. Phys. **23**, 385 (1990).

[9] T. Andersen, Phys. Rep. **394**, 157 (2004).

[10] D. J. Pegg, Nucl. Instrum. Methods Phys. Res., Sect. B **99**, 140 (1995).

[11] H. Bethe, in *Quantenmechanik der Einund Zwei-Elektronenprobleme* edited by H. Geiger and K. Scheeel, Handbuch der Physik, Vol. 24, Part 1 (Springer, Berlin, 1933), pp. 273–560.

[12] J. Cooper and R. N. Zare, J. Chem. Phys. **48**, 942 (1968).

[13] J. Cooper and R. N. Zare, J. Chem. Phys. **49**, 4252 (1968).

[14] D. Hanstorp, C. Bengtsson, and D. J. Larson, Phys. Rev. A **40**, 670 (1989).

[15] E. P. Wigner, Phys. Rev. **73**, 1002 (1948).

[16] D. Khuseynov, C. C. Blackstone, L. M. Culberson, and A. Sanov, J. Chem. Phys. **141**, 124312 (2014).

[17] A. M. Covington, D. Calabrese, W. W. Williams, J. S. Thompson, and T. J. Kvale, Phys. Rev. A **56**, 4746 (1997).

[18] A. M. Covington, S. S. Duvvuri, E. D. Emmons, R. G. Kraus, W. W. Williams, J. S. Thompson, D. Calabrese, D. L. Carpenter, R. D. Collier, T. J. Kvale, and V. T. Davis, Phys. Rev. A **75**, 022711 (2007).

[19] H. Hultgren, M. Eklund, D. Hanstorp, and I. Y. Kiyan, Phys. Rev. A **87**, 031404(R) (2013).

[20] O. Windelius, A. Aguilar, R. C. Bilodeau, A. M. Juarez, I. Rebolledo-Salgado, D. J. Pegg, J. Rohlén, T. Castel, J. Welander, and D. Hanstorp, Nucl. Instrum. Methods Phys. Res., Sect. B **410**, 144 (2017).

[21] C. Diehl, K. Wendt, A. O. Lindahl, P. Andersson, and D. Hanstorp, Rev. Sci. Instrum. **82**, 053302 (2011).

[22] D. Hanstorp, Meas. Sci. Technol. **3**, 523 (1992).

[23] R. J. Peláez, C. Blondel, M. Vandevraye, C. Drag, and C. Delsart, J. Phys. B: At., Mol. Opt. Phys. **44**, 195009 (2011).

[24] S. I. S., Inc., www.simion.com, SIMION v8.1 (2013).

[25] M. Génévriez, X. Urbain, A. Dochain, A. Cyr, K. M. Dunseath, and M. Terao-Dunseath, Phys. Rev. A **94**, 023407 (2016).

[26] M. Crance, J. Phys. B: At., Mol. Opt. Phys. **21**, 3559 (1988).

[27] R. Mabbs, E. R. Grumbling, K. Pichugin, and A. Sanov, Chem. Soc. Rev. **38**, 2169 (2009).

[28] V. T. Davis, J. Ashokkumar, and J. S. Thompson, Phys. Rev. A **65**, 024702 (2002).

[29] D. Calabrese, J. Phys. B: At., Mol. Opt. Phys. **30**, 4791 (1997).

[30] R. Mabbs, E. Surber, and A. Sanov, J. Chem. Phys. **122**, 054308 (2005).

[31] W. W. Williams, D. L. Carpenter, A. M. Covington, and J. S. Thompson, Phys. Rev. A **59**, 4368 (1999).

[32] A. F. Starace, Handbuch der Physik **31**, 1 (1982).

[33] G. Aravind, A. K. Gupta, M. Krishnamurthy, and E. Krishnakumar, Phys. Rev. A **75**, 042714 (2007).

[34] A. Sanov, Annu. Rev. Phys. Chem. **65**, 341 (2014).

[35] E. R. Grumbling and A. Sanov, J. Chem. Phys. **135**, 164302 (2011).